Journal of Anatomy

J. Anat. (2019) **234**, pp376–383 doi: 10.1111/joa.12928

3D statistical model of the pelvic ring – a CT-based statistical evaluation of anatomical variation

Charlotte Arand,[1,2] Daniel Wagner,[2] Robert Geoff Richards,[1] Hansrudi Noser,[1] Lukas Kamer,[1] Takeshi Sawaguchi[3] and Pol M. Rommens[2]

[1]*AO Research Institute Davos, Davos, Switzerland*
[2]*Department of Orthopaedics and Traumatology, University Medical Center Mainz, Mainz, Germany*
[3]*Department of Orthopaedics and Joint Reconstructive Surgery, Toyama Municipal Hospital, Toyama, Japan*

Abstract

The pelvic ring is a highly complex construct with a central role for human stability and mobility. The observable interindividual differences in skeletal anatomy are caused by anatomical variation in the innominate bones as well as the sacrum, further to differences in the spatial arrangement of these bones to each other. The aim of this study was to generate a 3D statistical model of the entire pelvic ring in order to analyse the observed interindividual differences and anatomical variation. A series of 50 anonymized pelvic CT scans of uninjured Japanese adults [30 males, 20 females, average age of 74.9 years, standard deviation (SD) 16.9 years] were processed and analysed, resulting in a 3D statistical overall mean model and separate male and female mean models. Principal component analysis (PCA) of the overall statistical model predominantly showed size variation (20.39%) followed by shape variation (14.13%), and a variation of the spatial arrangement of the sacrum to the innominate bones in different anatomical peculiarities (11.39 and 8.85%). In addition, selected internal and external pelvic parameters were manually measured with the objective of further evaluating and quantifying the observed interindividual as well as the known sex-specific differences. A separate statistical model of the grey value distribution based on the given Hounsfield unit (HU) values was calculated for assessing bone mass distribution, thus an indication of bone quality utilizing grey values as a quantitative description of radiodensity was obtained. A consistent pattern of grey value distribution was shown, with the highest grey values observed between the sacro-iliac joint and the acetabulum along the pelvic brim. Low values were present in the sacral ala, in the area of the iliac fossa as well as in the pubic rami next to the symphysis. The present model allows a differentiated analysis of the observed interindividual variation of the pelvic ring and an evaluation of the grey value distribution therein. Besides providing a better understanding of anatomical variation, this model could be also used as a helpful tool for educational purposes, preoperative planning and implant design.

Key words: 3D model; anatomical variation; interindividual variability; pelvic ring; principal component analysis.

Introduction

The pelvic ring is a complex anatomical structure of central importance for human stability and mobility during upright stance and gait (Messina, 1966). Essentially, the pelvic ring mainly functions to transfer and distribute the force created by the weight of the upper body onto the legs, allowing steady stance and upright gait, as well as protecting the pelvic organs. The female pelvis has different requirements than that of males, because of pregnancy and giving birth, and thus has a different anatomy (Messina, 1966).

With the left and right innominate bones, each composed of ilium, ischium and pubis, and the sacrum forming the pelvic ring, there are three rather complex bone structures forming a circular unit. Variation in each of these bones, further to the spatial arrangement of the bones in relation to each other, influences the overall architecture of the pelvic ring. Therefore, precise knowledge and understanding of its anatomical and biomechanical characteristics is necessary for adequate decision-making and treatment in the case of trauma or in the presence of degenerative

Correspondence
Charlotte Arand, Department of Orthopaedics and Traumatology, University Medical Center Mainz, Langenbeckstraße 1, 55131 Mainz, Germany. E: charlotte.arand@unimedizin-mainz.de

Accepted for publication *25 November 2018*
Article published online *21 December 2018*

pathologies (Kapandji, 1999; Moriggl & Jea, 2009). In addition, the use of individualized implants and their cost–benefit ratio necessitates the assessment of interindividual differences and consideration of the range of anatomical variation in the pelvic ring. However, assessment and specification of the observed interindividual differences and variations remain difficult using traditional methods.

The objective of this study was to generate a 3D statistical model of the entire pelvic ring to improve the anatomical understanding of the three ring-building bones and their relation to each other, and to visualize their interindividual variation (Noser et al. 2010; Wagner et al. 2014; Lambert et al. 2016). Principal component analysis (PCA) and separate measurements of external and internal pelvic parameters were performed further to quantify and analyse the specifications and peculiarities of the observed variabilities (Wold et al. 1987; Wagner et al. 2014, 2017a; Gehweiler et al. 2017). CT grey values provided in Hounsfield units (HU) were used for the evaluation of bone mass distribution.

Material and methods

CT imaging data

A series of 50 anonymized pelvic CT scans of Japanese adults were included in this study. The collection consisted of 30 males and 20 females with a mean age of 74.9 years (26–90 years, SD 16.9; males 68.4 years, SD 16.4; females 80.3 years, SD 6.7 years). CT scans were obtained from postmortem specimens after approval of the local ethics committee. CT samples with radiographic signs of bone-related pathologies other than osteopenia, osteoporosis or osteoarthritis were excluded. A standard CT scanner (LightSpeed VCT, GE Healthcare, Chalfont St. Giles, UK) was used, applying a clinical standard CT protocol with a tube peak voltage of 120 kVp and the GE STANDARD reconstruction kernel. The voxel size was 0.63 x 0.63 x 0.63 mm in all scans. CT grey values were provided in Hounsfield units (HU). All data were available in DICOM-format (Digital Imaging and Communications in Medicine).

Processing of imaging data

CT scans were processed using AMIRA software (Amira version 6.0.0, FEI, Hillsboro, OR, USA). Image segmentation was accomplished separately for each bone, sacrum and the two innominate bones using a threshold-based image segmentation tool and a subsequent manual slice by slice control and correction in axial slices (Fig. 1). After the segmentation process, separate triangulated mesh surfaces were generated for each bone. To achieve anatomical correspondence and comparability, homologous anatomical landmarks (37 per innominate bone, 42 per sacrum) were manually positioned onto defined anatomical points on each surface such as bony prominences, i.e. the anterior superior iliac spine (ASIS), the edge of the lunate fossa of the acetabulum or the rudimental intervertebral disc spaces of the sacrum, in accordance with a method described by Wagner et al. (2014). Additional non-anatomical segment landmarks were placed at sites of high curvature (Fig. 2A). All landmarks were visually checked for accurate placement by a medical expert. The segment landmarks were subsequently recomputed automatically to obtain equally numbered and equidistant landmarks (Fig. 2B,D). In addition, 32 additional anatomical landmarks were positioned as floating landmarks without contact to the surface within the sacral canal and the sacral foramina to define the inner outline of the sacrum (Fig. 2C).

3D statistical surface modelling

The surface of a random innominate bone and its landmark profile were taken as a first reference. Its triangular mesh was warped onto each of the remaining innominate bone surfaces according to the homologous landmarks using thin-plate spline transformation (TPS) (Bookstein, 1989, 1993). Thereafter, a homologous mesh structure with an identical number and localization of triangles and vertices was computed for each single bone surface. The sacra were processed accordingly. Homology between right and left innominate bone was achieved by mirroring the reference of the innominate bone. Each surface model was then aligned to its reference using a non-scaled Procrustes fit based on the homologous mesh structure (Bookstein, 1993; Kamer et al. 2010; Noser et al. 2010). This procedure resulted in separate preliminary models of the left and right innominate bones as well as the sacrum. Each single bone model consisted of 50 000 vertices and 100 000 triangles per innominate bone, and 50 000 vertices and 100 064 triangles per sacrum. These three mean models were then reused as a reference and the homology computation was repeated, resulting in the final sub-models of the isolated bones. The three separate bone models were assembled, and an overall statistical model of the entire pelvic ring was computed. To address the sex-specific anatomical differences, separate male and female mean models were computed in addition to the overall mean model.

Modelling of 3D statistical bone mass

An analysis of the mean bone mass distribution was performed according to a method described by Kamer et al. using CT grey values given in HU (Kamer, 2016). A regular reference grid was computed within the overall mean model with an isotropic voxel edge length of 0.5 mm. Based on the anatomical homologous landmarks, the reference grid was warped to each surface model using TPS transformation so that each voxel included through the segmentation process could be referenced to a voxel within the mean shape. The mean HU value for each voxel was calculated to obtain a mean model of the grey value distribution of the entire pelvic ring. The results were visualized as CT slices in all three planes and as a three-dimensional model.

Analysis

PCA was performed on the overall statistical model. PCA represents a common and valid statistical modelling method which ranks the main types of variation in size and shape in order of decreasing variance (Heimann & Meinzer, 2009; Heimann et al. 2009; Kamer et al. 2010; Noser et al. 2010). Models corresponding to three SD units flanking the mean were calculated for the 1st to 5th principal components (PCs) to display the range of variation captured. The statistical overall mean is equivalent to the status of all PCs at a level zero SD.

Specified measurements of the external and internal pelvis were performed to quantify interindividual differences. The distances between the anterior superior iliac spines (ASIS) and the distance between the anterior inferior iliac spines (AIIS) were selected as

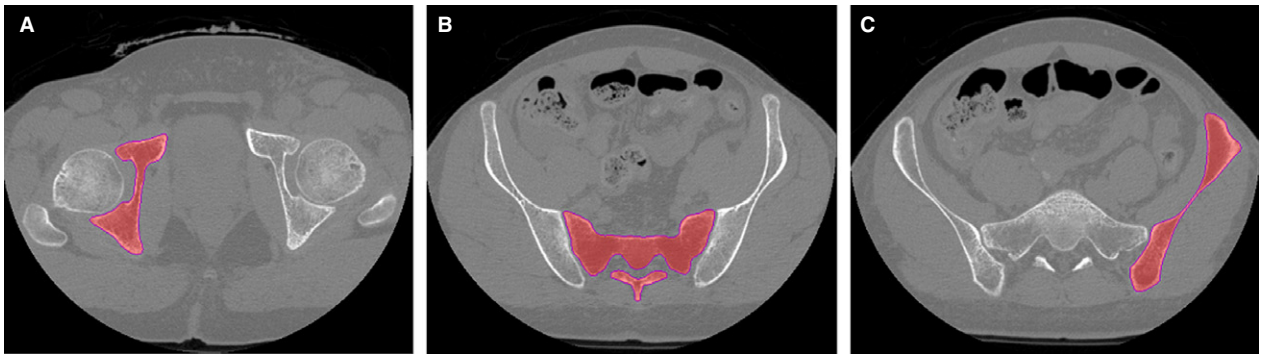

Fig. 1 Image segmentation. Threshold based semi-automated segmentation performed separately for the innominate bones (A, C) and the sacrum (B) in axial slices.

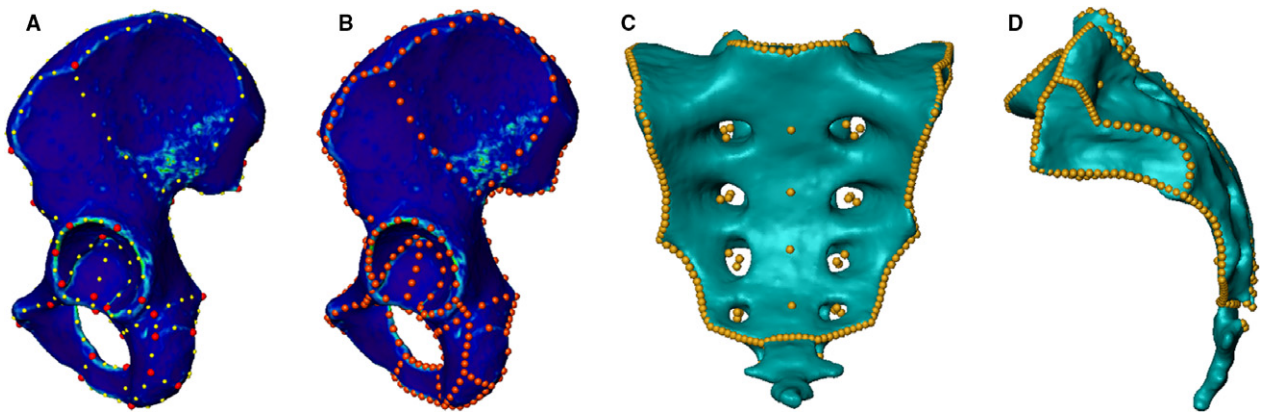

Fig. 2 Landmarking process. 3D surface models of a segmented innominate bone and a sacrum. The anatomical landmarks are represented by red dots and the segment landmarks by yellow dots shown on a left innominate bone in lateral view (A). The homologous landmarks on the same bone are represented by the orange dots (B). A complete homologous landmark set on a sacrum including surface landmarks and floating landmarks visualized in ap (C) and lateral (D) view.

external pelvic parameters. The distances between the promontory and the symphysis (conjugata vera) and the distance between the ischial spines were measured as internal pelvic parameters. These measurements were performed on the three mean models, the PCA results (1st–5th PCs, ± 3 SD) as well as on the original CT image datasets of all individual pelves included in the study using the AMIRA software. The Mann–Whitney U-test and Pearson correlation tests were applied on the final datasets using the SPSS software (IBM SPSS Statistics 24, IBM, Armonk, NY, USA).

To achieve a better visualization of the sex-specific differences, the male and female mean models were mutually aligned and a distance map was computed based on the homologous bone surfaces.

Results

A computer-generated 3D statistical model of the entire pelvic ring, including an overall as well as separate sex-specific mean models, and a 3D model of the bone mass distribution were successfully obtained. The statistical variation in size and shape was visualized and analysed using PCA. Major size and shape variation patterns were observed within the 1st to 5th PCs constituting 61.7% of the total anatomical variation. The 1st PC, representing the main variation, predominantly showed a difference in the pelvic size and contained 20.4% of the overall anatomical variation (Fig. 3). The distances between the ASIS, between the AIIS and between the promontory and the symphysis increased (+3 SD) and decreased (–3 SD), respectively, in the same manner. In contrast, the distance between the ischial spines showed an inverse behaviour to the other three parameters mentioned above. Shape differences were dominant in the 2nd PC (Fig. 4 D–I), which represented 14.1% of the total anatomical variation. A narrow pelvic inlet plane was observed to be associated with steep, nearly vertical iliac wings and a large cranio-caudal distance of the pubic rami. On the other side of the shape spectrum, laterally curved and overhanging iliac wings were seen together with a wide pelvic inlet plane and a lower height of the obturator foramen. The 3rd PC showed the major variation in the anterior-posterior position of the sacrum in relation to the innominate bone (11.4% of the overall anatomical variation). It varied from a posterior to an anterior position with a notable decrease of the distance between the

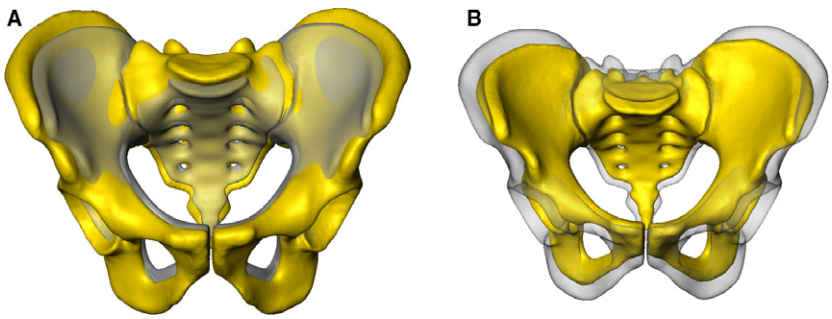

Fig. 3 1st PC Anatomical surface variation analysed using PCA: overall mean model in ap view, results of the 1st PC (yellow) in comparison with the mean in semi-transparent grey, +3 SD (A); −3 SD (B).

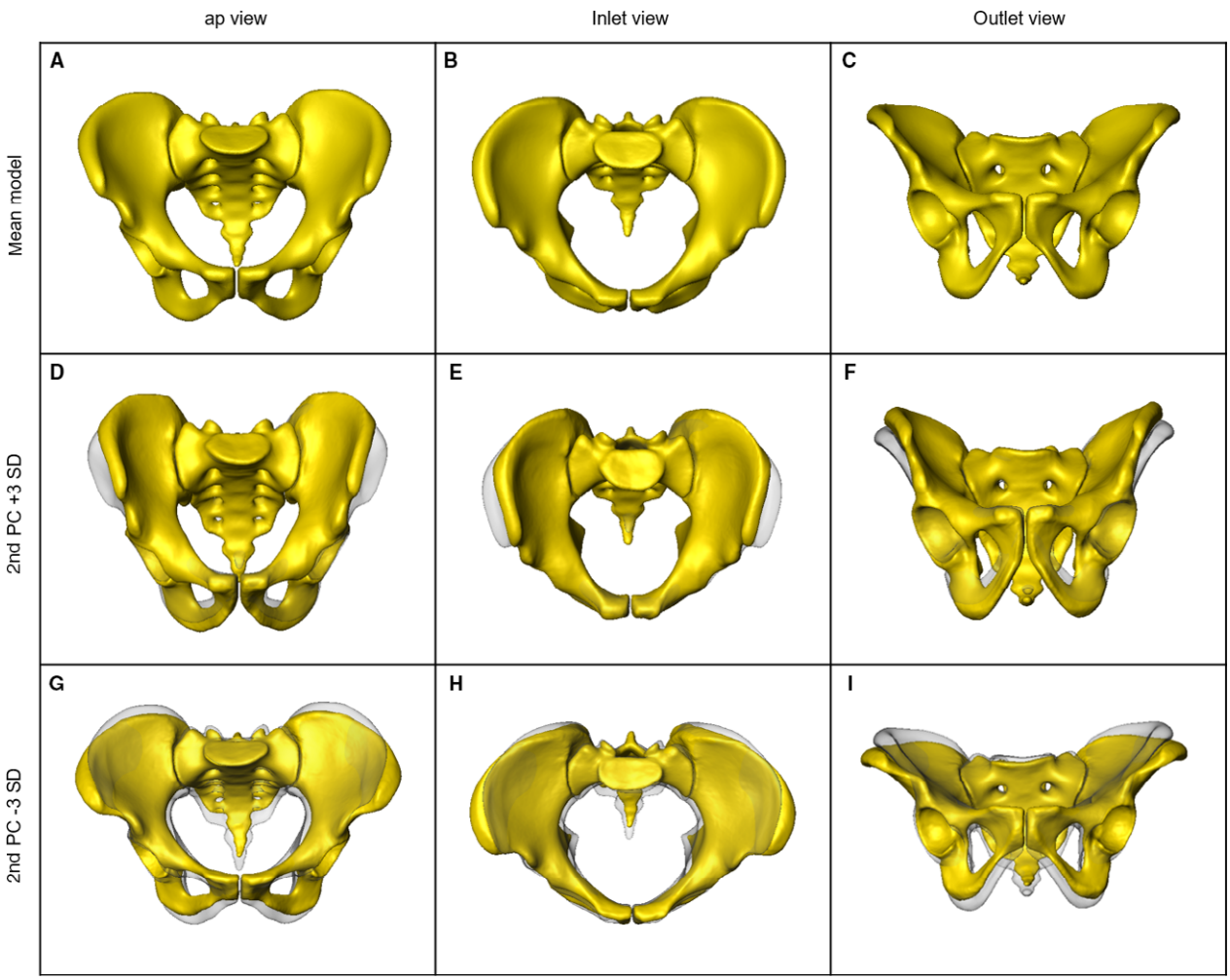

Fig. 4 2nd PC Anatomical surface variation analysed using PCA: overall mean model in ap, inlet and outlet view (A–C); results of the 2nd PC (±3 SD) in comparison to the mean in semi-transparent grey (D–I).

promontory and the symphysis. Concomitantly, the diameter of the S1 trans-sacral corridor was affected, decreasing with a more anterior positioning of the sacrum (Fig. 5A,B) (Wagner et al. 2014, 2017a). In the 4th PC, constituting 8.9% of the total anatomical variation, the observed changes are also dominated by the sacral position in relation to the innominate bone. The sacrum varied in its cranio-caudal position relative to the innominate bone. Here, a clear influence of the trans-sacral corridor of S1 in terms of size and availability was visible (Fig. 5C,D) (Wagner et al.

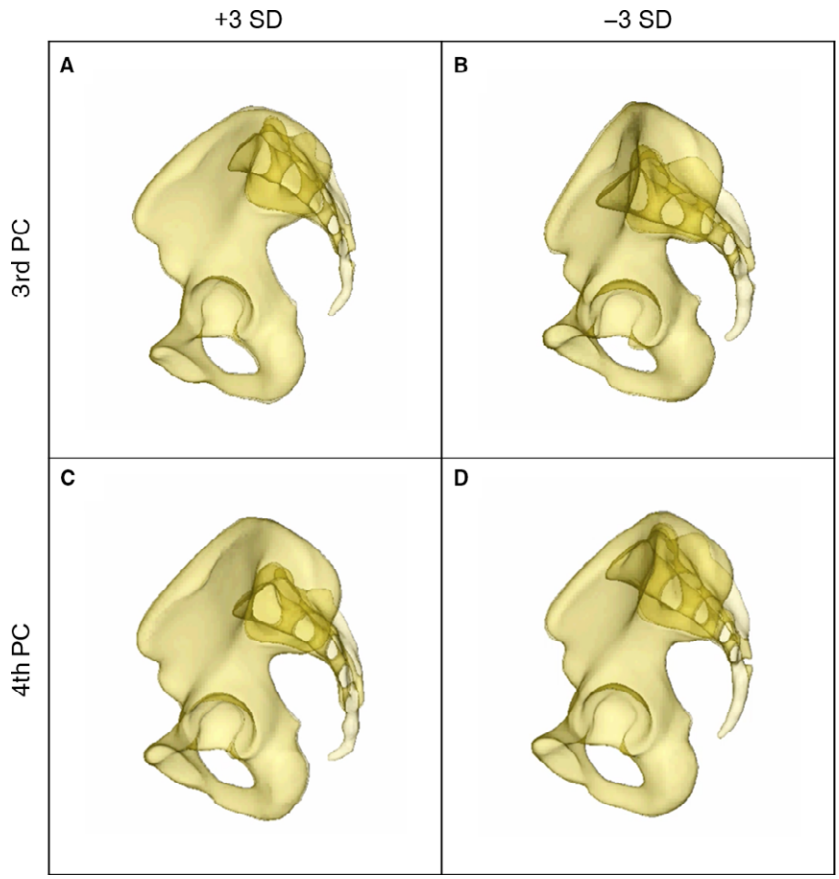

Fig. 5 3rd and 4th PC. Observed variation of the sacrum in relation to the innominate bone in 3rd [+3 SD (A), −3 SD (B)] and 4th PC [+3 SD (C); −3 SD (D)].

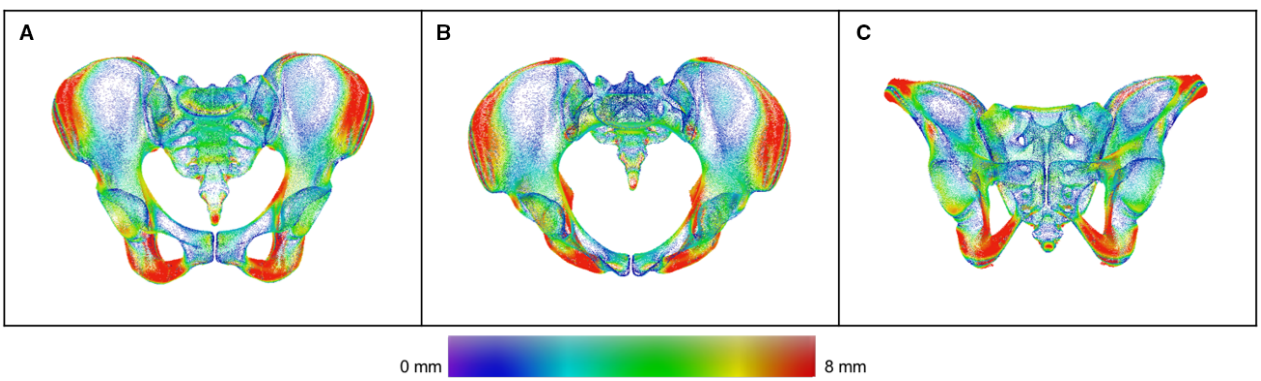

Fig. 6 Distance map between male and female mean. Color-coded distance map between the male and the female mean model in ap (A), inlet (B) and outlet view (C). Areas of higher sex related differences are displayed in red.

2014, 2017a). The 5th PC, constituting 6.9% of the total anatomical variation, predominantly presented variations in the sacral morphology, transforming from a long, rather straight sacrum in an almost vertical position in relation to the innominate bones to a rather short, more curved and inclined sacrum.

The separate male and female mean models were aligned and a distance map was calculated as illustrated in Fig. 6 showing the absolute value of differences. Maximum distance deviations were observed in the iliac wings, in the area of the ischial spine, in the ischial tuberosity and in the inferior pubic rami.

Analysis of the internal pelvic parameters exhibited higher values in the female pelvic models than in the male ones (Table 1). The distance between promontory and symphysis was measured at 107.3 mm in the male and

Table 1 Measurements of the internal and external pelvic parameters.

Distance	Promontory – symphysis (mm)	Ischial spines (mm)	ASIS (mm)	AIIS (mm)
Overall mean model	111.3	98.4	237.7	190.0
Median all samples SD (CI)	113.011.1 (110.7–116.9)	96.69.6 (95.7–101.1)	235.316.0 (233.2–242.3)	189.011.6 (186.7–193.2)
Male mean model	107.3	94.2	234.1	192.6
Median all male samplesSD (CI)	108.611.9 (107.5–116.4)	94.99.4 (93.3–100.3)	234.616.8 (229.9– 242.4)	192.2*10.6 (188.3– 196.3)
Female mean model	112.1	106.8	239.0	185.7
Median all female samplesSD (CI)	118.89.5 (112.2–121.1)	100.79.7 (96.3–105.4)	236.614.7 (233.2–247.0)	184.9*12.4 (180.6–192.3)

Measurements of the internal and external pelvic parameters on the overall mean, the gender-specific mean models. Values marked with * showed a significant sex-specific variation ($P < 0.05$). Standard deviation (SD), 95% confidence interval (CI).

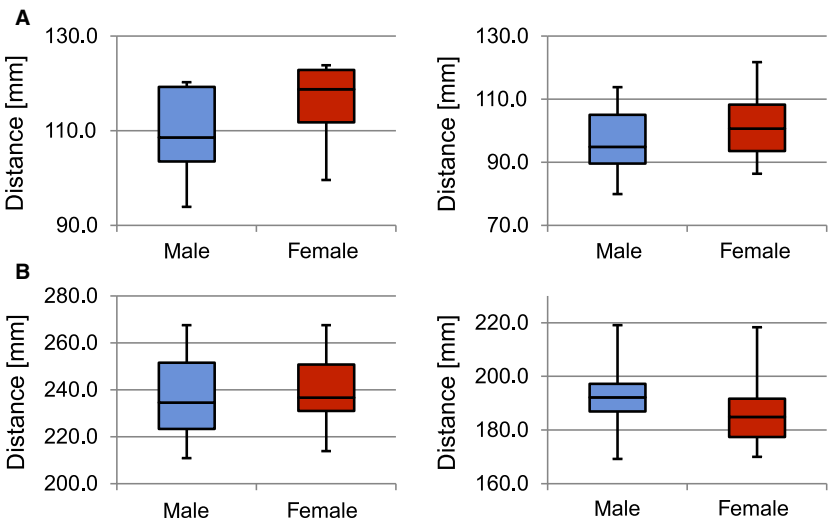

Fig. 7 Measurements of internal and external pelvic parameters. (A) Internal pelvic parameters: distance promontory – symphysis (mm), $P = 0.12$ (left); distance between the ischial spines (mm), $P = 0.2$ (right). (B) External pelvic parameters: distance between the anterior superior iliac spines (mm), $P = 0.38$ (left); distance between the anterior inferior iliac spines (mm), $P = 0.03$ (right).

112.1 mm in the female mean model, respectively. The largest intersexual differences of > 10 mm were observed between the ischial spines (94.2 mm in male, 106.8 mm in female, $P = 0.2$) (Fig. 7A). The external pelvic parameters also showed high interindividual variability (Fig. 7B). In the Mann–Whitney U-test performed on the 50 individual datasets, none of the observed sex specific differences was shown to be significant except for the distance between the AIIS, which was significantly smaller in female than in male pelves ($P = 0.03$). The Pearson correlation showed a positive correlation of the distance between ASIS and the distance between AIIS ($r = 0.54$, $P < 0.001$) as well as of the distance between ASIS and the distance between the ischial spines ($r = 0.42$, $P = 0.002$).

Evaluation of the 3D bone mass mean model showed a distinct and symmetrical pattern of grey value distribution. Areas of highest CT grey values were located between the sacro-iliac joint and the acetabulum along the pelvic brim (Fig. 8). Regions of intermediate bone mass were found periacetabular in the anterior and posterior column, the anterior and posterior wall and the area of the sacral body S1. Low CT grey values were observed in the sacral ala, the area of the fossa iliaca and the pubic rami next to the symphysis (Fig. 8).

Discussion

3D statistical modelling is a common and reliable method to analyse bone anatomy and the interindividual variations therein. It allows for a statistical evaluation of the observed variations (Radetzki et al. 2013; Sarkalkan et al. 2014; Gehweiler et al. 2017). The computation of pelvic models has been reported previously by several authors. Most of them used 3D models of individual pelves for preoperative planning (Noser et al. 2011; Bohme et al. 2012; Shim et al. 2017). Lamecker et al. (2004a,b) generated a 3D statistical

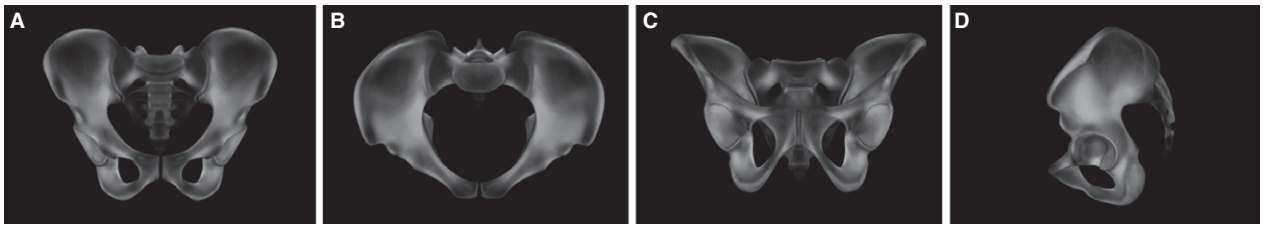

Fig. 8 Gray value distribution. 3D reconstruction of grey value distribution in the overall mean model in ap (A), inlet (B), outlet (C) and lateral view (D).

model of the pelvic ring based on 23 CT datasets with a focus on the technical workflow without considering the innominate bone and sacrum as separate structures or the sacral foramina. To the best of our knowledge, this is first study to demonstrate the generation of a CT-based 3D statistical model of the entire pelvic ring including all sacral foramina and canals as well as grey value distribution. Based on this model, further analysis was performed using PCA, allowing analysis of specifications and peculiarities of the known interindividual differences in the bone anatomy of the pelvic ring. The predominant variation was shown to be the variation in bone size, followed by shape variation occurring particularly in the innominate bone. Internal and external pelvic parameters were measured on the three mean models and on each sample to quantify and analyse further the observed variations. The internal parameters most prominently showed characteristic sex-specific differences, with higher values measured in the female samples. Taking into account the special role of the female pelvis during pregnancy and childbirth, the observed differences of the internal parameters represent a meaningful evolutionary development meeting biological and anatomical demands. By comparing the observed shape variations in the 2nd PC with the measurements of the internal and external pelvic parameters, it can be assumed that the 2nd PC shows predominantly sex-related shape variations. This assumption is strengthened by the comparison of the male and the female mean models (Fig. 6), which shows a similar pattern of differences to that observed in the 2nd PC. Nevertheless, even if the observed anatomical differences present distinct characteristics of males and females, these differences were surprisingly small when measured, and no sex-related significance could be shown except for the distances between the AIIS. A reason for this might be the predominance of interindividual variation, especially in size, over sex-related variation. Although not available at the present time, a correlation with body height would be an interesting parameter to consider in future studies.

Furthermore, a high variability in the spatial arrangement of the three main bone structures of the pelvic ring was observed (3rd and 4th PC). The position of the sacrum in relation to the innominate bones was found to vary relevantly. Wagner et al. (2014, 2017a,b) showed a high variability in the trans-sacral corridor S1 and its accessibility pertinent to the ilio-sacral screw and trans-sacral bar fixation, respectively. The results of the present study show that not only the morphology of the sacrum itself but also the shape of the innominate bone and the spatial interarrangement of the bones affect the size and accessibility of the trans-sacral corridor.

Grey value distribution showed a consistent pattern of high HU values along the pelvic brim between the sacroiliac joint and the acetabulum, and regions of low HU values in the sacral ala (corresponding to the so-called alar void described by Peretz et al. 1998; Ebraheim et al. 2000; Rommens, 2017), iliac wing and in the pubis rami next to the symphysis without relevant sex-specific differences. These findings provide valuable information not only about fracture care when considering preoperative planning and screw positioning, but also for planning endoprosthetic joint replacement. In particular, in the case of revision surgery with exchange of prostheses, an exact knowledge of the bone stock distribution is essential for adequate and sufficient anchoring of the prosthesis.

Conclusion

The pelvic ring presents very high interindividual variability in size and shape as well as spatial arrangement of the ring-building bones, considering that the first five PCs cover only 61.64% of the observed overall variation. The 3D model described in the current study can be a helpful tool for further investigations of shape and grey value distribution when considering optimization of pre-existing and development of new implants for fracture treatment, especially in terms of screw positioning and plate design for treating acetabular fractures. Furthermore, this 3D model could provide valuable information in planning endoprosthetic joint replacement, particularly for revision surgery. The model also lays down the platform for further analysis of special areas of interest by creating sub-models, for example for the sacro-iliac joint. In addition, this 3D model could be instrumental in teaching and in improving understanding of the pelvic anatomy.

Acknowledgements

We acknowledge the support of Dr. Karsten Schwieger. This study was co-funded by the TK System of the AO Foundation, Davos, Switzerland, and by DePuy Synthes, Zuchwil, Switzerland. Charlotte

Arand received a research fellowship grant from the AO Research Institute Davos, Davos, Switzerland.

Author contributions

Charlotte Arand: corresponding author, study design, data processing, analysis and interpretation, manuscript. Daniel Wagner: initiation and concept of the project, critical revision of the manuscript. Robert Geoff Richards: contribution to concept, infrastructure, critical revision of the manuscript. Hansrudi Noser: study design, data processing, critical revision of the manuscript. Lukas Kamer: initiation of the project, contribution to concept and study design, data acquisition, critical revision of the manuscript, approval of the article. Takeshi Sawaguchi: initiation of the project, data acquisition, critical revision of the manuscript. Pol M. Rommens: initiation of the project, data interpretation, critical revision of the manuscript, approval of the article.

References

Bohme J, Shim V, Hoch A, et al. (2012) Clinical implementation of finite element models in pelvic ring surgery for prediction of implant behavior: a case report. *Clin Biomech* **27**(9), 872–878.

Bookstein FL (1989) Principal warps: thin-plate splines and the decomposition of deformations. *IEEE Trans Pattern Anal Mach Intell* **11**(6), 567–585.

Bookstein FL (1993) Morphometric tools for landmark data: geometry and biology. *Q Rev Biol* **68**(4), 293–368.

Ebraheim N, Sabry FF, Nadim Y, et al. (2000) Internal architecture of the sacrum in the elderly. An anatomic and radiographic study. *Spine* **25**(3), 292–297.

Gehweiler D, Wahnert D, Meier N, et al. (2017) Computational anatomy of the dens axis evaluated by quantitative computed tomography: implications for anterior screw fixation. *J Orthop Res* **35**(10), 2154–2163.

Heimann T, Meinzer HP (2009) Statistical shape models for 3D medical image segmentation: a review. *Med Image Anal* **13**(4), 543–563.

Heimann T, van Ginneken B, Styner MA, et al. (2009) Comparison and evaluation of methods for liver segmentation from CT datasets. *IEEE Trans Med Imaging* **28**(8), 1251–1265.

Kamer L (2016) Computational anatomy of the proximal humerus: An ex vivo high-resolution peripheral quantitative computed tomography study. *J Orthop Translat* **4**, 46–56.

Kamer L, Noser H, Schramm A, et al. (2010) Orbital form analysis: problems with design and positioning of precontoured orbital implants: a serial study using post-processed clinical CT data in unaffected orbits. *Int J Oral Maxillofac Surg* **39**(7), 666–672.

Kapandji IA (1999) *Funktionelle Anatomie der Gelenke Bd. 3: Rumpf und Wirbelsäule*. Stuttgart: Hippokrates.

Lambert S, Al-Hadithy N, Sewell MD, et al. (2016) Computerized tomography based 3D modeling of the clavicle. *J Orthop Res* **34**(7), 1216–1223.

Lamecker H, Seebass M, Hege H-C, et al., eds (2004a) A 3D statistical shape model of the pelvic bone for segmentation. Proc. SPIE 5370, Medical Imaging 2004: Image Processing; (2004) https://doi.org/10.1117/12.534145

Lamecker H, Seebass M, Lange T, et al. (2004b) Visualization of the variability of 3D statistical shape models by animation. *Stud Health Technol Inform* **98**, 190–196.

Messina N (1966) The bony pelvis I. Anatomy and signs of physiodynamics. *Rass Int Clin Ter* **46**(10), 505–520.

Moriggl B, Jea WC (2009) Becken – Funktionelle Anatomie. *Praxis der Orthopädie und Unfallchirurgie*, pp. 629–631. Stuttgart: Thieme.

Noser H, Hammer B, Kamer L (2010) A method for assessing 3D shape variations of fuzzy regions and its application on human bony orbits. *J Digit Imaging* **23**(4), 422–429.

Noser H, Radetzki F, Stock K, et al. (2011) A method for computing general sacroiliac screw corridors based on CT scans of the pelvis. *J Digit Imaging* **24**(4), 665–671.

Peretz AM, Hipp JA, Heggeness MH (1998) The internal bony architecture of the sacrum. *Spine* **23**(9), 971–974.

Radetzki F, Mendel T, Noser H, et al. (2013) Potentialities and limitations of a database constructing three-dimensional virtual bone models. *Surg Radiol Anat* **35**(10), 963–968.

Rommens PM (2017) *Fragility fractures of the pelvis*. 1st edn. New York: Springer.

Sarkalkan N, Weinans H, Zadpoor AA (2014) Statistical shape and appearance models of bones. *Bone* **60**, 129–140.

Shim V, Hoch A, Grunert R, et al. (2017) Development of a patient-specific finite element model for predicting implant failure in pelvic ring fracture fixation. *Comput Math Methods Med* **2017**, 9403821.

Wagner D, Kamer L, Rommens PM, et al. (2014) 3D statistical modeling techniques to investigate the anatomy of the sacrum, its bone mass distribution, and the trans-sacral corridors. *J Orthop Res* **32**(11), 1543–1548.

Wagner D, Kamer L, Sawaguchi T, et al. (2017a) Critical dimensions of trans-sacral corridors assessed by 3D CT models: Relevance for implant positioning in fractures of the sacrum. *J Orthop Res* **35**(11), 2577–2584.

Wagner D, Kamer L, Sawaguchi T, et al. (2017b) Morphometry of the sacrum and its implication on trans-sacral corridors using a computed tomography data-based three-dimensional statistical model. *Spine J* **17**(8), 1141–1147.

Wold S, Esbensen K, Geladi P (1987) Principal component analysis. *Chemometr Intell Lab Syst* **2**(1), 37–52.